nature structural & molecular biology



# A peptide motif in Raver1 mediates splicing repression by interaction with the PTB RRM2 domain

Alexis P Rideau[1], Clare Gooding[1], Peter J Simpson[2], Tom P Monie[3], Mike Lorenz[4], Stefan Hüttelmaier[5], Robert H Singer[6], Stephen Matthews[2], Stephen Curry[3] & Christopher W J Smith[1]

**Polypyrimidine tract–binding protein (PTB) is a regulatory splicing repressor. Raver1 acts as a PTB corepressor for splicing of α-*tropomyosin* (*Tpm1*) exon 3. Here we define a minimal region of Raver1 that acts as a repressor domain when recruited to RNA. A conserved [S/G][I/L]LGxxP motif is essential for splicing repressor activity and sufficient for interaction with PTB. An adjacent proline-rich region is also essential for repressor activity but not for PTB interaction. NMR analysis shows that LLGxxP peptides interact with a hydrophobic groove on the dorsal surface of the RRM2 domain of PTB, which constitutes part of the minimal repressor region of PTB. The requirement for the PTB-Raver1 interaction that we have characterized may serve to bring the additional repressor regions of both proteins into a configuration that allows them to synergistically effect exon skipping.**

Interest in the mechanisms underlying regulated alternative splicing has intensified in recent years because of its role in expanding the protein-coding capacity of genomes[1]. Alternative splicing is controlled by enhancer and silencer elements, located in exons and introns, that activate or repress splicing[2,3]. Splicing enhancers commonly bind activator proteins of the SR family, whereas splicing silencers often bind repressor heterogeneous nuclear ribonucleoproteins (hnRNPs). PTB (also known as hnRNP-I and PTBP1) is one of the better-studied splicing repressor proteins (reviewed in ref. 4). Structurally, it consists of four RNA-recognition motif (RRM)-type domains, all of which bind RNA[5–7]. The optimal binding sequence corresponds to known splicing silencers[8]. Exons repressed by PTB usually have at least two high-affinity binding sites for PTB. One of these is often associated with the polypyrimidine tract (PPT), but additional sites can be present upstream of the branchpoint[9], in the exon[10,11] or in the downstream intron[12,13]. PTB can compete with U2AF65 binding at the PPT[14,15], but its action at other sites seems to be more complex. PTB repression of the *SRC* N1 exon involves cooperative binding of PTB to high-affinity sites flanking the exon[16]. Cooperative binding is consistent with early suggestions that PTB is dimeric[17,18], but more recent biophysical data demonstrate that pure PTB is monomeric[6,9,19], and structural models for cooperative binding without PTB-PTB interaction have been suggested[7].

PTB is widely expressed, and in many cell types it acts as a repressor[4]. Regulation requires PTB-mediated repression to be relieved in particular cell types. For example, CELF proteins[20–22] can functionally antagonize PTB, sometimes by binding competitively to adjacent sites. Replacement of PTB by one of its tissue-restricted paralogs, nPTB[23,24], ROD1 (ref. 25) or smPTB in rodents[26], is another mechanism. nPTB is less repressive for *SRC* N1 exon splicing than PTB, and it also promotes assembly of an enhancer complex downstream of the exon[24]. Another means for modulating PTB activity is via corepressors.

Raver1 was initially identified in yeast two-hybrid screens for binding partners of the cytoskeletal protein vinculin[27] but was also found to interact with PTB and to be localized in either the cytoplasm or nucleus[27]. Raver1 has three RRMs at the N-terminal end and an extended C-terminal region containing a proline-rich region (**Fig. 1**). Cotransfection of Raver1 with *Tpm1* constructs leads to a switch in splicing of the mutually exclusive exons 2 and 3 toward greater inclusion of the smooth muscle–specific exon 2 (ref. 28). This effect occurs by repression of exon 3 and depends upon PTB-binding silencers flanking exon 3. Artificial tethering experiments have shown that the function of the downstream silencer (DY) can be replaced by recruitment of PTB, Raver1 or just the Raver1 C-terminal region (residues 442–748). Yeast two-hybrid and *in vitro* pull-down experiments indicate that the N-terminal half of Raver1 (residues 1–441) mediates interactions with PTB[27,28]. This has suggested a model in which *Tpm1* splicing is regulated by the PTB-mediated recruitment of a splicing repressor domain of Raver1.

We set out to further analyze the splicing repressor and PTB-binding activity of Raver1 using artificial tethering experiments and fluorescence resonance energy transfer (FRET) microscopy *in vivo*, and pull-downs and NMR *in vitro*. Splicing repressor activity is

[1]Department of Biochemistry, University of Cambridge, 80 Tennis Court Road, CB2 1GA, UK. Divisions of [2]Molecular Biosciences and [3]Molecular and Cell Biology, Imperial College, South Kensington Campus, Exhibition Road, London SW7 2AZ, UK. [4]Max Planck Institute of Molecular Cell Biology and Genetics, Pfotenhauerstr. 108, 01307 Dresden, Germany. [5]Medical Faculty, University of Halle-Wittenberg, Heinrich-Damerow-Str. 1, 06907 Halle (Saale), Germany. [6]Department of Anatomy & Structural Biology, Albert Einstein College of Medicine, 1300 Morris Park Avenue, Bronx, New York 10461, USA. Correspondence should be addressed to C.W.J.S. (cwjs1@cam.ac.uk).

Received 3 March; accepted 27 July; published online 27 August 2006; doi:10.1038/nsmb1137

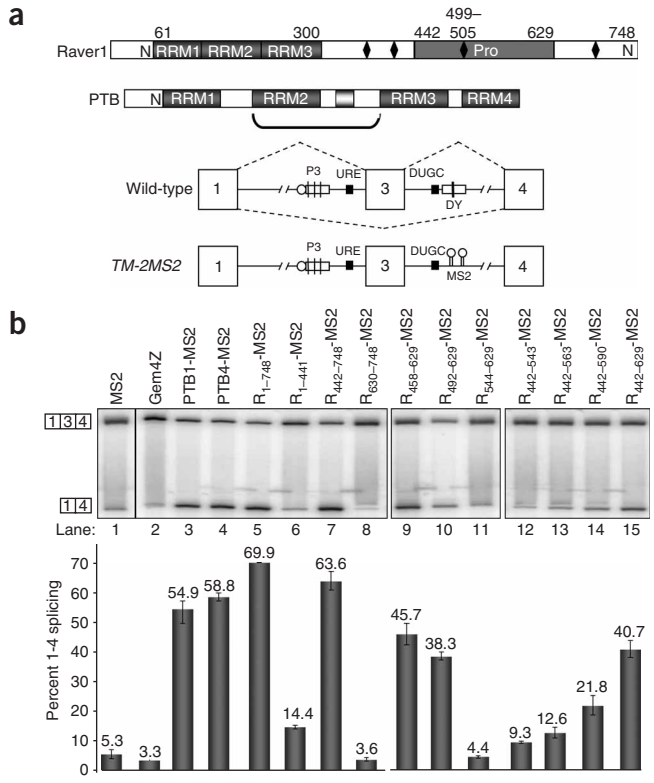


**Figure 1** A proline-rich splicing repressor domain in Raver1. (**a**) Schematic representation of domain structures of Raver1 and PTB and of *Tpm1* splicing reporters. RRMs and proline-rich region of Raver1 are indicated. N, nuclear-localization signals; black diamonds, PTB-interacting peptides identified in this study. The initially identified peptide is at 499–505; others are at 360–66, 400–406 and 684–690. The wild-type splicing reporter has exons 1, 3 and 4 of *Tpm1*. Regulated skipping of exon 3 is mediated by regulatory elements P3, URE, DUGC and DY. In construct *TM-2MS2*, the PTB-binding DY element is replaced by two binding sites for bacteriophage MS2 coat protein. (**b**) RT-PCR of *TM-2MS2* cotransfected into PAC-1 cells with the various effectors indicated above. Histogram shows percent regulated exon skipping ± s.d.

contained within the proline-rich region encompassing residues 492–629. Furthermore, PTB binding is not restricted to the N-terminal half, as three nonoverlapping regions of Raver1 can interact with PTB, including the minimal repressor domain. We identified a previously uncharacterized peptide motif with a core sequence [S/G][I/L]LGxxP (where x is potentially any residue) that is both necessary for splicing repression and sufficient for PTB interaction, and that occurs four times in Raver1. Interaction of the peptide with PTB was analyzed by NMR, revealing specific contacts with the α-helical side of RRM2. Moreover, RRM2 was capable of forming a ternary complex by binding simultaneously to RNA and Raver1 peptide on opposite sides of the domain. Notably, RRM2 constitutes part of the essential minimal repressor domain of PTB identified by MS2 tethering[29]. The PTB-binding motif is found in other proteins and may represent a general motif for PTB cofactors.

## RESULTS

### Minimal repressor domain

To define the minimal region of Raver1 that has splicing repressor activity, we used artificial recruitment by the MS2 coat protein. In the reporter construct *TM-2MS2*, the DY PTB-binding element is replaced by two adjacent MS2-binding sites (**Fig. 1a**), leading to a low level of exon 3 skipping in transfected PAC1 smooth muscle cells (**Fig. 1b**, lane 2). Splicing repression can be restored by cotransfection of MS2 coat protein fused to PTB or Raver1 (lanes 3–5), and it remains dependent upon the remaining *cis*-regulatory elements and is regulated by cell type[28,29]. As previously observed[28], cotransfection with MS2 fusion proteins containing full-length Raver1 ($R_{1–748}$-MS2, lane 5) or $R_{442–748}$-MS2 (lane 7) led to substantial levels (>60%) of exon skipping. In contrast, $R_{1–441}$-MS2 had a much lower activity (lane 6), even though this region is sufficient for interaction with PTB[27,28]. The C-terminal region contains a proline-rich region between residues 442 and 629. $R_{442–629}$-MS2 retained substantial repressor activity (~40% exon skipping, lane 15), whereas the remainder of the C-terminal region was inactive ($R_{630–748}$-MS2, lane 8). Further deletions from the N-terminal end of the 442–629 fragment showed that repressor activity was retained in 458–629 and 492–629 fragments but was lost upon deletion to 544–629 (lanes 9–11). In contrast, additional deletions from the C-terminal end of 442–629 were accompanied by a progressive loss of activity (lanes 12–15). Western blots using the Flag epitope in the MS2 fusion protein showed that all proteins were expressed to similar levels (data not shown). Together, these data indicate that a minimal repressor domain is contained within 138 residues between positions 492 and 629. According to two-hybrid data, this region cannot interact with PTB[27]. However, activity of $R_{442–629}$-MS2 was substantially reduced when the upstream PTB-binding sites in the P3 pyrimidine tract were mutated (**Supplementary Fig. 1** online), suggesting that the repressor domain remains dependent upon PTB.

### Three PTB-interacting regions

Concurrent with mapping the repressor domain, we aimed to further characterize the PTB-interacting region, which was thought to lie within $Raver1_{300–400}$ (ref. 28). Various *in vitro*–translated Raver1 fragments were assayed in glutathione *S*-transferase (GST)-PTB pull-downs (**Fig. 2a**). Consistent with previous data, full-length Raver1 was pulled down (lanes 9 and 10), whereas the RRM-containing $Raver1_{1–307}$ was not (lanes 11 and 12). $Raver1_{1–455}$ was pulled down with GST-PTB, but only in the absence of RNase treatment (lanes 13 and 14). There are various possible explanations for the RNase sensitivity (see Discussion), but we note that two-hybrid, FRET and NMR analyses indicate a stable and specific interaction of $Raver1_{1–455}$ with PTB (see ref. 27 and results below). $Raver1_{300–455}$ also bound weakly with RNase sensitivity (lanes 15 and 16). Two more nonoverlapping fragments, $Raver1_{456–563}$ and $Raver1_{564–748}$, also bound PTB in the absence of RNase treatment (lanes 23–26), even though two-hybrid assays had detected no interaction between PTB and $Raver1_{442–748}$ (ref. 27). Raver1 constructs containing at least two of the above three nonoverlapping fragments bound stably to PTB with little or no RNase sensitivity (lanes 17–22).

Interaction of Raver1 fragments with PTB was analyzed *in vivo* by FRET between cotransfected cyan fluorescent protein (CFP)-tagged PTB and yellow fluorescent protein (YFP)-tagged Raver1 (**Fig. 2b** and **Table 1**). Substantial nuclear FRET signals were observed with full-length Raver1 and $Raver1_{1–455}$, in both the nucleoplasm and the perinucleolar compartments (PNCs). To compare different experiments and expression levels, the observed FRET signals were normalized[30]. N-terminally tagged full-length Raver1 and $Raver1_{1–455}$ had identical normalized FRET (nFRET) signals (**Table 1**), as the N terminus

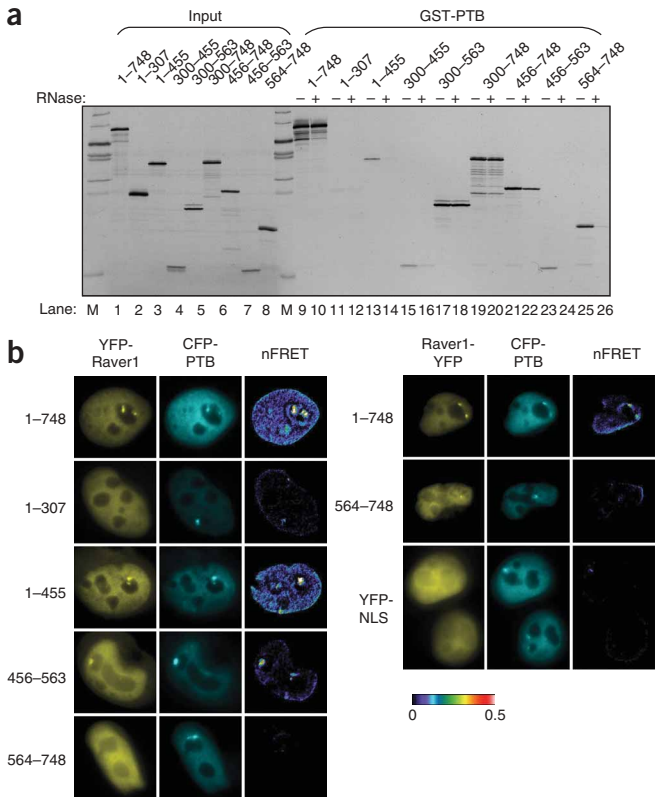


**Figure 2** Multiple PTB-interacting regions of Raver1. (**a**) Raver1 fragments indicated above lanes were translated *in vitro* (lanes 1–8), then pulled down with GST-PTB (lanes 9–24) either with (+) or without (–) prior RNase treatment. (**b**) FRET analyses of the association of PTB and Raver1 in HeLa cells. YFP-fused full-length (1–748) Raver1 and fragments (indicated at left) were coexpressed with CFP-PTB. nFRET denotes normalized FRET (see Methods). **Table 1** shows the nFRET values for each YFP-fusion protein in both the PNC and the nucleoplasm. Full-length Raver1 fused N- or C-terminally to YFP showed an energy transfer indicating an association with PTB. As a negative control, YFP was fused to a nuclear-localization signal (NLS) only. The C-terminal fragment $Raver1_{1–455}$ bound PTB, whereas a shorter fragment (1–307) and the N terminus (567–745) did not. The $Raver1_{455–563}$ fragment also interacted with PTB.

remained unchanged and, thus, the orientation and/or distance to CFP should be the same. FRET efficiency was lower when YFP was moved to the C terminus of full-length Raver1, indicating the distance sensitivity of this photophysical effect. Energy transfer was also observed with $Raver1_{456–563}$ but not with $Raver1_{564–748}$ To exclude the possibility that the loss of FRET of the C-terminal fragment is due to a distance and/or orientation change between the two fluorophores, YFP was fused to the C terminus of $Raver1_{564–748}$ and that of full-length $Raver1_{1–748}$. Whereas the full-length construct showed substantial FRET in PNCs, no energy transfer was observed with $Raver1_{564–748}$-YFP, indicating that the C-terminal region of Raver1 does not bind PTB in PNCs. As expected, $Raver1_{1–307}$ was also negative for PTB binding. The FRET data therefore confirm that at least two regions of Raver1 (1–455 and 456–563) can interact with PTB *in vivo*, and the pull-down data additionally suggest a third region (564–748) able to interact with PTB. Notably, the minimal repressor domain (492–629) overlaps the 456–563 and 564–748 PTB-interacting fragments.

### A PTB-interacting peptide

Alignment of the proline-rich region of four Raver1 orthologs revealed the sequence 496-PGVSLLGEPPKD-507 to be fully conserved, apart from two conservative substitutions in *Xenopus laevis*. Notably, this sequence was present in the active construct 492–629 but absent in 544–629, which had no repressor activity (**Fig. 1b**). To assess the functional importance of residues 496–507, we carried out alanine-scanning mutagenesis within the parental construct $R_{442–629}$-MS2 (**Fig. 3a**, lane 15). A related construct, $R_{511–629}$-MS2, designed to remove the conserved sequence by N-terminal truncation, had severely impaired repressor activity (lane 14) and served as a negative control. Alanine substitutions at Ser499, Leu500, Leu501, Gly502 and Pro505 reduced repressor activity to levels comparable to $R_{511–629}$-MS2. Mutations at Pro496, Gly497 and Val498 had no effect, whereas mutations at Glu503, Pro504, Lys506 and Asp507 had very modest effects. Western blots confirmed that all proteins were expressed at comparable levels (**Fig. 3b**). These data therefore demonstrate that the motif SLLGxxP is important for the splicing repressor activity of $R_{442–629}$-MS2. We next tested whether the alanine-scanning mutations affected the ability to interact with PTB. Raver1-MS2 proteins were transcribed and translated *in vitro* (**Fig. 3c**, upper gel) and pulled down with either GST-PTB (center gel) or GST-SXL (lower gel). As expected, $Raver1_{442–629}$ bound PTB, whereas $Raver1_{511–629}$ was pulled down much less efficiently. The alanine-scanning mutants showed similar detrimental effects upon PTB binding as in the splicing-repression assay. Substitution of Leu500, Leu501 and Gly502 markedly impaired PTB binding. P505A had a modest effect, but the double mutant P504A P505A reduced binding even further. These data confirm that the motif 500-LLGxxP-505 is important for interaction of Raver1 with PTB and for the splicing repressor activity of Raver1. Moreover, the C-terminal deletion mutants of the repressor domain (**Fig. 1b**, lanes 12–15) were all pulled down equally well with PTB (data not shown), despite their progressive loss of splicing repressor activity. Together with the data in **Figure 3**, this indicates that interaction with PTB via the 500–505 motif is necessary but not sufficient for activity of the Raver1 repressor domain and that additional repressor function resides in residues 512–629.

To probe the interaction of PTB with the Raver1 motif in greater detail, two further constructs were made containing the essential motif within a 21-residue ($R_{491–511}$-MS2) or 12-residue ($R_{496–507}$-MS2) context. Both proteins interacted with PTB, but the 21-residue construct bound more efficiently. We carried out further mutagenesis in the context of the 21-residue construct (**Fig. 4a**). Each residue from Val498 to Pro505 was substituted by alanine. In addition, Ser499 was

**Table 1 Normalized FRET values for CFP-PTB and YFP-Raver1 fusion proteins in the perinucleolar compartment and the nucleoplasm**

| Raver1 fusion | Perinucleolar compartment | Nucleoplasm |
|---|---|---|
| YFP-$Raver1_{1–748}$ | 0.47 ± 0.12 | 0.10 ± 0.03 |
| YFP-$Raver1_{1–307}$ | 0.03 ± 0.04 | 0.03 ± 0.02 |
| YFP-$Raver1_{1–455}$ | 0.44 ± 0.10 | 0.11 ± 0.04 |
| YFP-$Raver1_{456–563}$ | 0.30 ± 0.07 | 0.05 ± 0.03 |
| YFP-$Raver1_{564–748}$ | 0.04 ± 0.05 | 0.04 ± 0.02 |
| $Raver1_{1–748}$-YFP | 0.32 ± 0.06 | 0.04 ± 0.03 |
| $Raver1_{564–748}$-YFP | 0.05 ± 0.04 | 0.01 ± 0.01 |
| YFP-NLS | 0.04 ± 0.05 | 0.02 ± 0.01 |

Errors shown are s.d.

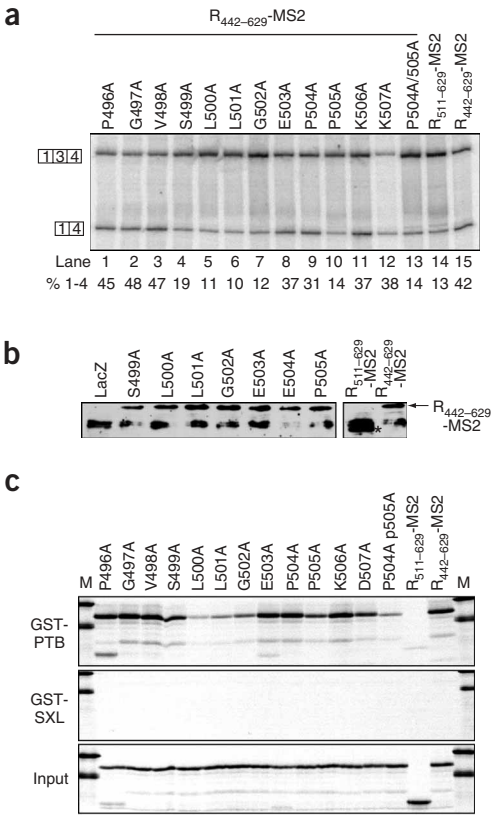


**Figure 3** A peptide motif essential for splicing repression and PTB binding. (**a**) RT-PCR analysis of splicing of *TM-2MS2* in PAC-1 cells after cotransfection with the effectors indicated above the lanes. Apart from $R_{511–629}$-MS2 (lane 14), all effectors had Raver1 (R) residues 442–629 fused to MS2, with the indicated alanine-scanning mutations at positions 496–505. Percent exon skipping is listed below lane numbers. (**b**) Western blot of wild-type $R_{442–629}$-MS2 and of the mutants with impaired splicing activity in **a**. LacZ is a mock control transfection. Arrow, $R_{442–629}$-MS2 proteins; asterisk, $R_{511–629}$-MS2. (**c**) Constructs used in **a** were transcribed and translated *in vitro* (input), then pulled down with either GST-PTB or GST-SXL. Mutations that impaired splicing repression in **a** had a similar effect upon PTB binding. M, size marker.

mutated to aspartate (to mimic phosphoserine) and glycine, and Leu500 and Leu501 were both mutated to the other aliphatic–side chain residues, isoleucine and valine. Of the alanine mutations, V498A, E503A and P504A had no effect, whereas S499A, L500A, L501A, G502A and P505A reduced PTB binding, correlating well with the splicing-repression data. Of the additional substitutions at Ser499, the aspartate mutant (S499D) did not bind, whereas S499G retained PTB-binding activity. Substitution of leucine by isoleucine had no effect at Leu500, but impaired activity at Leu501. Substitution by valine at either position abolished binding. The double proline mutant P504A P505A impaired PTB binding more severely than P505A. Together, these data suggest that [S/G][I/L]LGxxP is a consensus PTB-binding motif.

In addition to the 499-SLLGEPP-505 motif, three additional sequences in mouse Raver1 match this consensus: 360-GLLGAPP-366, 400-GILGDSP-406 and 684-GLLGLGP-690 (**Fig. 4b**). Notably, each of the Raver1 fragments that was pulled down with GST-PTB (**Fig. 2**) contained one or two of these motifs. We also noted a similar motif (PLLGDHP) at position 277 in hnRNPL, a known PTB-interacting protein[31]. The four Raver1 motifs and the hnRNPL motif were tested as 20-residue peptides in pull-down assays, along with a Leu→Ala mutant of each (**Fig. 4c**). All the motifs except for $Raver1_{677–696}$ were pulled down with GST-PTB, and in each case the Leu→Ala mutation impaired this interaction. However, only the motif at 353–372 was pulled down with an efficiency matching that of $Raver1_{491–511}$. These data indicate that Raver1 has at least three PTB-interacting motifs and that similar motifs in other proteins may also mediate interaction with PTB.

To test the functional importance of the PTB-binding motifs, we introduced alanine mutations into positions 2, 3, 4 and 7 of the four [S/G][I/L]LGxxP motifs in Raver1 and compared the ability of the mutant protein to bind PTB and to regulate *Tpm1* splicing (**Fig. 5**). As expected, the mutant protein was not pulled down with GST-PTB (**Fig. 5a**). Although expressed to comparable levels (**Fig. 5c**), the mutant Raver1 had a reproducibly reduced effect upon *Tpm1* exon 3 skipping (**Fig. 5b**), confirming the importance of the PTB-interacting motifs for splicing regulation by Raver1.

## Raver1 peptide interacts with PTB RRM2

We used NMR spectroscopy to examine the Raver1-binding site in PTB. Titration of synthetic $Raver1_{491–511}$ peptide with $^{15}$N-labeled

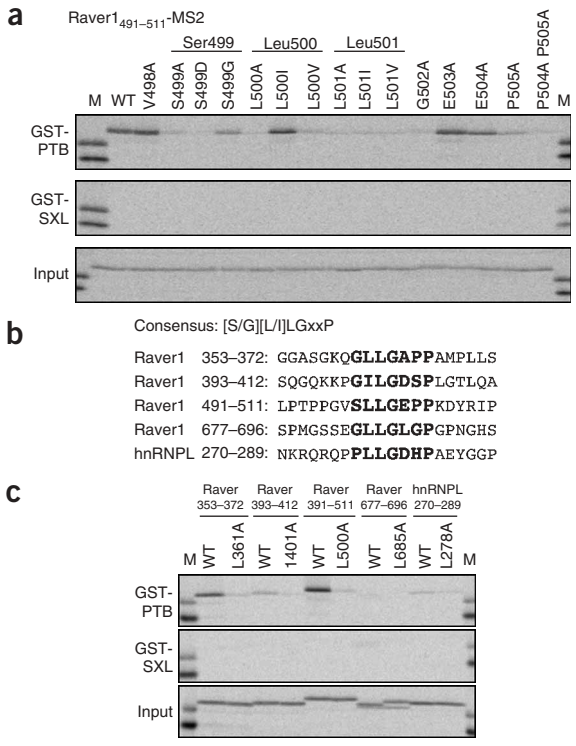


**Figure 4** [S/G][L/I]LgxxP is sufficient to bind PTB. (**a**) The 20-residue $Raver1_{491–511}$ peptide, fused to MS2, was transcribed and translated *in vitro* (input) and then pulled down with GST-PTB or with GST-SXL as a control. Effects of single mutations indicated above gels were also tested. (**b**) Consensus PTB-interacting motif derived from **a** is shown with three more motifs in Raver1 and one in hnRNPL that all conform to the consensus. (**c**) GST-PTB pull-down of 20-residue peptides encompassing each of the four motifs in Raver1 and the motif in hnRNPL. Each motif was expressed as a fusion with MS2 and was tested as wild-type and with an alanine mutation at the second position of the motif.

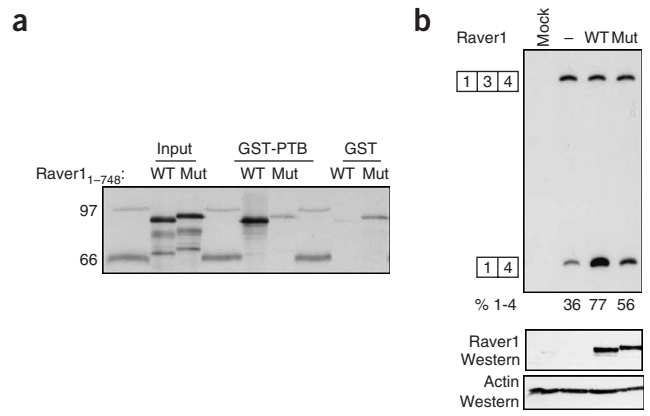


**Figure 5** Mutation of the four PTB-binding motifs impairs Raver1 activity. (**a**,**b**) Mutant full-length Raver1 in which all four potential PTB-interacting motifs were mutated to alanine at positions 2, 3, 4 and 7 (relative to start of motif) was tested alongside wild-type Raver1 in a GST-PTB pull-down (**a**) and a cotransfection with wild-type *Tpm1* splicing reporter (**b**). Splicing in **b** was analyzed by RT-PCR, and percent exon skipping is listed below the lanes. (**c**) Western blot for Raver1 and actin of the same four samples as in **b**. Lanes in **b** and **c** are aligned.

PTB constructs PTB1-1234 (full-length PTB1 lacking the N-terminal 55 residues), PTB1-12 (residues 55–301, encompassing RRM1 and RRM2) and PTB1-34 (residues 335–531, encompassing RRM3 and RRM4) was monitored by 2D $^{1}$H-$^{15}$N HSQC. All of these PTB constructs revealed changes in chemical shifts located solely within RRM2 (data not shown). To reduce signal overlap and map the interaction more precisely, the titration was repeated with PTB1-2, a construct comprising RRM2 only (residues 177–286)[6]. 2D $^{1}$H-$^{15}$N HSQC spectra recorded with increasing peptide concentration revealed chemical shift changes for a number of residues on the α-helical face of the RRM (**Fig. 6**). Substantial shifts were observed in Leu191–Val195 within the loop connecting strand β1 with helix α1, Asp198–Gln202 at the N-terminal end of α1 and Leu241–Leu253 within the extended region connecting α2 with β4. Notably, the binding site is on the opposite face from the site of RNA interaction[6,7], suggesting that RRM2 could bind Raver1 and RNA simultaneously (see below).

The binding affinity of the Raver1 peptide for a variety of PTB constructs containing RRM2 was measured by NMR shift titration. Changes in chemical shift measured with increasing peptide concentration were fit to a standard single–binding site saturation isotherm for constructs PTB1-2, PTB1-12, PTB1-23 (residues 147–433, encompassing RRM2 and RRM3) and PTB1-2L and PTB4-2L (comprising RRM2 plus the entirety of the C-terminal linker to RRM3 from PTB isoforms 1 (residues 147–334) and 4 (residues 147–360), respectively). All constructs had essentially the same affinity for the Raver1 peptide, within experimental error ($K_d \approx$ 60–135 μM, **Supplementary Fig. 2** online). Together, the data indicate that the helical face of RRM2 provides the sole interaction interface on PTB for this Raver1 motif. Furthermore, titration of PTB1-12 with the 19-residue Raver1$_{353–371}$ peptide (encompassing the GLLGAPP motif) revealed a similar pattern of shift changes on the helical face of RRM2 and bound with a similar affinity ($K_d \approx$ 180 μM, **Supplementary Fig. 2**).

To investigate the specificity of the observed interaction, we titrated PTB1-2 with a Raver1$_{491–511}$ peptide containing the L500A mutation that severely impaired pull-down with GST-PTB (**Figs. 3** and **4**). Appreciable shift changes were observed only with a large excess of the L500A peptide (10–100 molar equivalents; data not shown), revealing a dramatic drop in affinity ($K_d$ estimated to be >3 mM). The titration was also repeated with an 8-residue peptide, SLLGEPPK, encompassing only the central (499–506) region of Raver1$_{491–511}$. The peptide bound with only a modestly lower affinity ($K_d \approx$ 200 μM) than the longer Raver1$_{491–511}$ construct (**Supplementary Fig. 2**) and with an essentially identical pattern of NMR shift changes across the RRM2 surface. Despite the small reduction in affinity, these observations confirm that the consensus [S/G][I/L]LGxxP sequence is the primary element responsible for specific interaction with PTB.

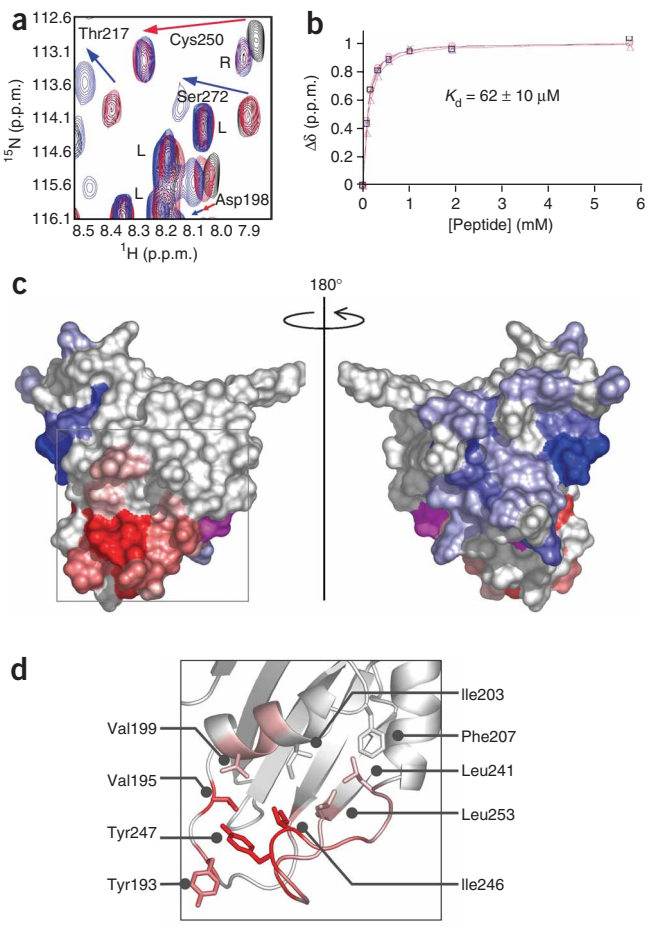


**Figure 6** Interaction of Raver1$_{491–511}$ and RNA with PTB RRM2. (**a**) Region of the 2D $^{1}$H-$^{15}$N HSQC spectrum of PTB1-2 in the absence (black) and presence (red) of excess Raver1 peptide (LPTPPGVSLLGEPPKDYRIP) and with subsequent addition of 5 molar equivalents of RNA ligand (blue). Some peaks undergoing appreciable shift changes are highlighted by red (Raver1 addition) and blue (RNA addition) arrows; R* indicates a natural abundance signal from the peptide; L indicates unassigned amide signals from the PTB1 interdomain linker. (**b**) Fit of a binding isotherm for the Raver1 peptide titration. Normalized change in NMR chemical shift (Δδ) is plotted against peptide concentration. Mean fit $K_d$ ± s.d. from five different amide shifts is indicated. (**c**) Surface representation of RRM2 with color gradients showing shift changes upon Raver1 addition (white, no change; red, largest change) and subsequent RNA addition (blue, largest change). Residues whose resonances are affected by both ligands are colored magenta. Shift changes are the weighted sum 7 × Δδ($^{1}$H) + Δδ($^{15}$N). (**d**) Close-up of boxed region in **c**. Hydrophobic and aromatic residues lining the putative shallow Raver1-binding groove are indicated.

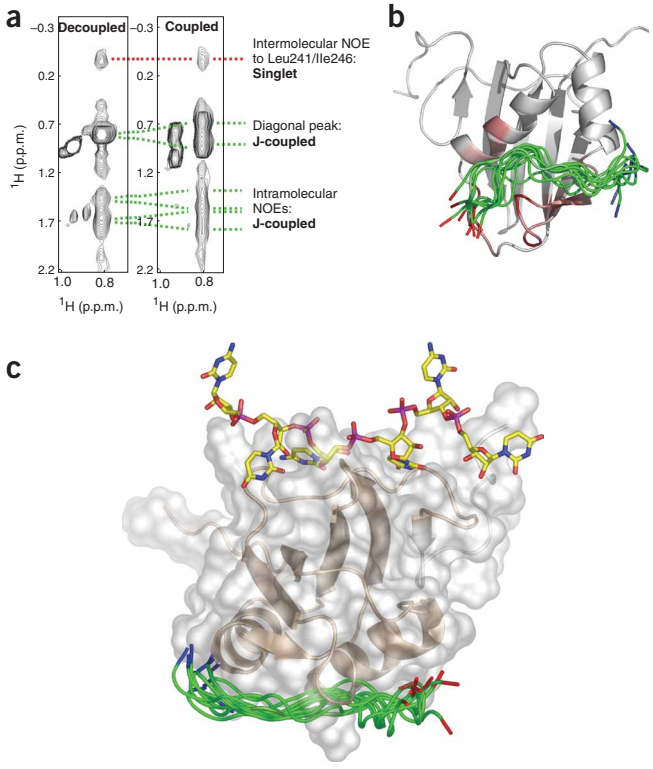


**Figure 7** Structural model of the complex of Raver1 peptide with PTB RRM2. (**a**) Strip plots taken from J-decoupled and J-coupled $^{13}$C-separated NOESY-HSQC spectra of the RRM2–Raver1$_{496–507}$ complex, showing NOEs from the side chain methyl groups of Raver1 Leu500 and Leu501. The multiplet structure used to differentiate intermolecular from intramolecular NOEs is indicated. (**b**) Family of structures of the RRM2–Raver1$_{496–507}$ complex derived from HADDOCK docking. Average RRM2 structure (cartoon representation, colored according to shift change upon Raver1$_{491–511}$ addition as in **Fig. 6c**) and conformation of the Raver1 motif (green ribbon) is shown for the ten lowest-energy models from cluster 1. Direction of the peptide is indicated by color (blue, N terminus; red, C terminus). (**c**) Model of the RRM2–Raver1–RNA ternary complex, derived from the published structure of the RRM2–RNA complex[7] (PDB entry 2ADB) and the cluster of docked RRM2–Raver1 structures. RRM2 is shown as a cartoon and surface representation, Raver1 peptide backbone as a green ribbon and RNA as yellow sticks.

### RRM2 forms a ternary complex with RNA and Raver1

The observation that RRM2 interacts with Raver1 on the opposite face from the RNA-binding site suggests that the domain may be able to interact with both ligands simultaneously, forming a ternary complex. To verify this, a sample of PTB1-2 saturated with 50 molar equivalents of Raver1$_{491–511}$ peptide was titrated with the RNA oligonucleotide 5′-CUUCUCUCU-3′, a PTB-binding sequence found upstream of the *SRC* N1 exon[9]. A number of NMR chemical shift changes upon RNA addition were observed in residues comprising the known RNA-binding site of RRM2 (refs. 6,7), whereas residues implicated in Raver1$_{491–511}$ binding showed little or no perturbation from their chemical shift in the bound state (**Fig. 6a,c** and **Supplementary Fig. 3** online). The pattern of shift changes upon RNA binding was essentially identical to that observed in the titration in the absence of Raver1$_{491–511}$ (**Fig. 6a,c** and ref. 6). Furthermore, the affinity of RRM2 for RNA, as determined by NMR ($K_d \approx 10$ μM, **Supplementary Fig. 2**), was unchanged from that reported in the absence of Raver1 peptide[6]. These data confirm that PTB1 RRM2 can interact simultaneously with RNA and the Raver1$_{491–511}$ motif to form a ternary complex.

### Structural model for the RRM2–Raver1 motif complex

To elucidate the structural details of the PTB RRM2-Raver1 interaction, NMR studies were performed on a 1:1 complex of PTB1-2 with a $^{15}$N,$^{13}$C-labeled Raver1$_{496–507}$ peptide (496-PGVSLLGAPPKD-507, labeled residues underlined). To maximize the expected number of observable intermolecular NOEs, we replaced the centrally located Glu503 with alanine, which provides the improved spectral properties of the side chain methyl group while not affecting affinity (**Figs. 3** and **4**; confirmed by NMR, data not shown). Unfortunately, backbone amide signals from residues Leu500–Ala503 (inclusive) in Raver1$_{496–507}$ were not visible in $^1$H-$^{15}$N HSQC spectra of the saturated complex (20-fold excess of RRM2) and were severely attenuated at stoichiometric ratios (**Supplementary Fig. 4** online), owing to line broadening caused by conformational exchange on the ms–μs timescale. Despite this, methyl-group signals were observable in $^1$H-$^{13}$C HSQC spectra of the Raver1$_{496–507}$–RRM2 complex, which suggests that although the peptide backbone experiences conformational exchange these key side chains do not.

To explore the interaction in greater detail, we attempted to measure intermolecular NOEs between side chains of Raver1$_{496–507}$ and the PTB1-2 RRM domain. NOEs are measurable if the interatomic distance, averaged over the conformational ensemble, is short ($<5$ Å). It is therefore notoriously difficult to measure intermolecular NOEs in weak complexes, as they are often not represented by a unique bound conformation and can be averaged. To maximize sensitivity, we used a standard 3D $^{13}$C-NOESY-HSQC spectrum to measure NOEs between Raver1$_{496–507}$ and the RRM. Two spectra were recorded in the presence and absence of $^{15}$N-$^{13}$C decoupling in the indirect $^1$H dimension, enabling NOEs to be assigned to protons that are not coupled to a heteronucleus (that is, predominantly intermolecular NOEs from labeled Raver1$_{496–507}$ to unlabeled PTB1-2). Intermolecular NOEs could be unambiguously assigned between side chains within the core region of Raver1$_{496–507}$ and the helical face of PTB1-2 (**Fig. 7a**). Specifically, 11 intermolecular NOEs were identified from the side chain methyl groups of Raver1 Leu500, Leu501 and Ala503 to several methyl- and aromatic-containing side chains on the helical face of the RRM. The presence of intermolecular NOEs for these residues provides evidence for direct interaction of the core [I/L]LGx motif with the RRM and highlights the importance of these residues in binding PTB.

The presence of severe conformational exchange and the low affinity of the interaction indicated that it would not be feasible to determine a high-resolution structure of the complex by standard methods. Nevertheless, the clear delineation of a binding interface using chemical shift mapping and the intermolecular NOE data enabled us to adopt an NMR restraint–guided docking approach (HADDOCK) to generate a representative ensemble of structures for the complex in solution[32]. Standard ambiguous interaction restraints (AIRs[32]), based on NMR chemical shift mapping of both the PTB1-2 RRM and the Raver1 peptide, together with the 11 measured intermolecular NOEs, were used to restrain the calculation (see Methods). The 200 final refined structures for the PTB1-2–Raver1 complex were clustered according to a pairwise r.m.s. deviation cutoff of 1.5 Å, producing one major and three minor clusters of 117, 25, 16 and 11 structures. The average intermolecular energies of the ten best structures from each cluster were –142 ± 29, –111 ± 18, –119 ± 31 and –111 ± 41 kcal mol$^{-1}$, respectively. In all clusters, the peptide was

found to lie in the shallow binding groove on the helical face of RRM2. Additionally, the direction of the peptide backbone is identical in all structures (see below); the clusters differ by small changes in backbone conformation.

**Figure 7b** shows an overlay of the ten lowest-energy, water-refined models from cluster 1. Our ensemble of structures for the Raver1 motif–PTB interaction reveals a number of important features. As suggested by the chemical shift mapping data, the Raver1 motif binds in the shallow groove formed primarily between helix α1 and residues 241–248 from the extended loop region linking helix α2 with strand β4 of PTB RRM2. Within this groove, the peptide was consistently found to lie in the same direction, which in the orientation shown is right to left (N- to C-terminal; **Fig. 7b**). This orientation is consistent with the observation that truncation of the Raver1$_{491–511}$ peptide to the core peptide (Raver1$_{499–506}$) perturbs the chemical shifts assigned to the side chain amide protons of Gln244 (predicted to be proximal to the N terminus; **Supplementary Fig. 5** online). Furthermore, it is supported by paramagnetic relaxation enhancement data from N-terminally spin-labeled core peptides, which were found to specifically affect Gln244 (**Supplementary Fig. 5**).

The binding site can accommodate at least 9 residues of peptide in an extended conformation, and in the docked complex it spans Raver1 residues Gly497–Pro505 (inclusive), encompassing the [S/G][I/L]LGxxP motif highlighted by the GST pull-down and NMR titration data. The shallow binding groove is lined with a number of hydrophobic residues (**Fig. 6d**), and the hydrophobic packing of the prominent 500-Leu-Leu-501 motif on Raver1 against the helical face of RRM2 is important in the interaction (**Supplementary Fig. 6** online). In all the structures from the final ensemble, the side chain of Leu501 is more buried than Leu500, which perhaps explains the lack of tolerance for mutation of Leu501, whereas Leu500 can be replaced with isoleucine without disrupting the interaction. Our model of the complex is completely consistent with the functional data presented in this report and will facilitate the design of mutagenesis experiments to probe the molecular aspects of the PTB-Raver1 interaction in greater detail.

## DISCUSSION

Our data provide important new insights into structural and functional aspects of splicing repression by PTB and its corepressor Raver1. We set out to identify an effector domain of Raver1 that could repress splicing when recruited via MS2. We expected repressor function to be separable from PTB- or RNA-binding functions, which were thought to lie entirely within Raver1$_{1–442}$ (refs. 27,28). However, the repressor domain (442–629) required the 499–505 PTB-interacting peptide. The site of interaction with PTB is within RRM2 (**Figs. 6** and **7**), which, along with the following inter-RRM linker, constitutes the minimal repressor domain of PTB when recruited by MS2 (ref. 29). Notably, the minimal repressor domain of each protein contains one module that interacts with the other repressor domain, as well as an additional essential repressor region—residues 511–629 of Raver1 and the inter-RRM linker adjacent to PTB RRM2. Thus, the requirement for the 499-SLLGEPP-505 interaction with RRM2 may serve to bring the two additional repressor modules into apposition, thereby facilitating their functional synergy in promoting exon skipping. This is consistent with the involvement in many splicing regulatory complexes of multiple cooperative interactions between regulators, coregulators and RNA[33].

The PTB-binding peptide motif from Raver1 binds the helical face of RRM2, thus allowing the domain to simultaneously interact with protein and RNA ligands. The mode of interaction seems to be similar to the binding of a peptide motif from SF1 to the third RRM domain of U2AF65 (ref. 34). In this case, binding of the SF1 peptide strongly depends on insertion of a tryptophan side chain into a hydrophobic cleft between the two helices on the dorsal face of the RRM; the conserved leucine residues at positions 2 and 3 of the Raver1 motif may have a similar role in binding PTB-RRM2. The fact that PTB RRM2 can interact simultaneously with both the Raver1 peptide and RNA (**Fig. 7c**) indicates that the both Raver1 and RNA may be molecular targets of the RRM2 part of the minimal PTB repressor domain. Future work will test the relative importance of these interactions by mutagenesis targeted to key residues in the RNA- and Raver1-binding sites of RRM2.

Binding of the peptide to RRM2 is relatively weak ($K_d \sim 100$ μM), which might account for the relatively inefficient RNase-sensitive pull-down of some Raver1 fragments (**Fig. 2**). RNase sensitivity is usually taken as evidence against a direct protein-protein interaction and is attributed to the fact that both proteins bind a common RNA. However, the NMR data clearly demonstrate that short LLGxxP peptides interact specifically with RRM2 in the absence of RNA. Moreover, Raver1 fragments that individually bound PTB with RNase sensitivity bound stably and independently of RNase when combined within a single polypeptide. This could be explained by avidity effects in the GST-PTB pull-down (**Fig. 2a**). Therefore, although the basis of RNase-sensitive pull-down remains unclear, in this case it does not indicate an indirect RNA-bridged interaction.

Our data demonstrate the importance of the interaction between PTB RRM2 and the SLLGEPP motif in Raver1. The additional essential repressor regions of the two proteins do not provide additional PTB-Raver1 contacts. C-terminal deletions from Raver1 residues 629–543 progressively impaired repressor activity (**Fig. 1b**) with no effect upon pull-down by GST-PTB (data not shown). Likewise, no interaction of the PTB linker region with Raver1 peptides was detected by NMR and there was no difference in the interaction of Raver1 peptide with PTB1 and with PTB4 (**Supplementary Fig. 2**), even though the minimal PTB4 repressor domain is more active than PTB1 (ref. 29). The additional repressor regions presumably have distinct molecular targets—either additional corepressors or components of the core splicing machinery. Recent reports on regulation of *SRC* and *FAS* exons suggest that PTB directly interferes in the interactions involved in exon or intron definition[11,35]. Artificially recruited PTB and Raver1 also repress the *FAS* exon[11]. It will be interesting to see whether the same minimal PTB and Raver1 repressor domains are active in this system. The implication would be that the proline-rich region of Raver1 or the linker between PTB RRM2 and RRM3, or both, may target core spliceosome components. Both the PTB and Raver1 repressor regions are proline rich and the Raver1 domain contains PxxP and PPLP motifs, which in other proteins mediate interactions with SH3 and WW domains, respectively[34]. Notably, the progressive loss of activity with the series of C-terminal deletions in the repressor domain (**Fig. 1b**, lanes 12–15) might be explained by the loss with each deletion of RxPxEPxL motifs. A noteworthy candidate spliceosomal target for proline-rich motifs is PRPF40A, which has a tyrosine-rich WW domain and is proposed to be involved in early bridging interactions between splice sites[36–38]. This is precisely the kind of target that might lead to interference with exon or intron definition[11,35]. Characterization of the additional essential repressor regions of Raver1 and their molecular targets is an important future goal and may explain why mutation of all four PTB-interacting motifs in full-length Raver1 impairs, but does not eliminate, splicing repressor activity (**Fig. 5**).

Irrespective of additional molecular targets, one possible role for Raver1 in regulating *Tpm1* splicing is to promote RNA looping

between the PTB-binding sites flanking *Tpm1* exon 3. Because it has up to four motifs that can interact with PTB, a single Raver1 molecule might be able to interact simultaneously with separate PTB molecules bound at the upstream P3 and downstream DY elements (**Fig. 1a**). Consistent with this model, the minimal PTB and Raver1 repressor domains recruited by MS2 downstream of exon 3 would also be capable of reconstituting a protein bridge to the upstream regulatory elements. Raver1$_{442–629}$-MS2 would be able to interact directly with PTB bound upstream of exon 3. The minimal repressor domain of PTB, which includes RRM2 (ref. 29), fused to MS2 could interact with a bridging Raver1 molecule that simultaneously contacts a second PTB molecule at the upstream site. *In vitro* analyses of the stoichiometry of Raver1-PTB interactions will help to address the feasibility of this model.

To date, *Tpm1* exon 3 is the only model system that is highly responsive to Raver1. In other PTB-regulated model systems like α-*actinin* and *PTB* exon 11, overexpressed Raver1 is less active than PTB or completely inactive[39]. Why does *Tpm1* exon 3 need a Raver1 corepressor, whereas in other systems PTB alone is sufficient? A clue might lie in the 460-nucleotide (nt) separation of the PTB-binding elements flanking *Tpm1* exon 3. Exon skipping is further decreased when these elements are moved apart[40]. By contrast, the PTB sites flanking the well-characterized *SRC* N1 exon are all contained within a region of ~120 nt, and repressive looping can occur without the need for cofactors[9,16]. An analogy for the proposed distance-related dependence upon a cofactor is found in the sex-specific splicing enhancer in the *Drosophila melanogaster doublesex* gene. This enhancer lies more than 300 nt from the 3′ splice site that it activates and requires the female-specific transformer protein as well as SR proteins for activity. However, when relocated closer to the 3′ splice site, it has constitutive enhancer activity in the absence of transformer[41].

We found variants of the initially identified PTB-binding motif elsewhere in Raver1, as well as in hnRNPL. A motif search of the SwissProt database using the query sequence [S/G][I/L]LGxPP identified Raver2, another known PTB-interacting protein (ref. 42 and C.G. and C.W.J.S., unpublished data). The Raver1 motifs at positions 500 and 360, which interacted most efficiently with PTB *in vitro*, are conserved in Raver2. Among other noteworthy proteins containing potential PTB-interaction motifs was Matrin3, with a conserved GILGPPP motif. In two-hybrid assays, both Matrin3 and PTB interacted with the RNA-binding protein Nova[23]. Potentially, Matrin3 could interact simultaneously with both Nova and PTB. Moreover, our mutagenesis of the PTB-interacting motif was not exhaustive, and we may have identified only a subset of related motifs that can bind PTB. Likewise, the surface of PTB RRM2 that interacts with the Raver1 peptide is conserved in the nPTB, ROD1 and smPTB paralogs (data not shown), so these paralogs are likely to interact with a similar spectrum of cofactors. We have demonstrated the functional relevance of the characterized interaction between PTB and the Raver1 cofactors in a single alternative splicing event. The potential for similar molecular interactions between all PTB paralogs and a range of cofactors suggests that many other PTB-regulated events in the nucleus and cytoplasm may also be modulated by similar interactions.

## METHODS

**Constructs, transfections, reverse-transcription PCR, westerns and pull-downs.** All molecular biology techniques followed standard protocols used previously[28]. Various regions of Raver1 were cloned into unique MluI and AvrII sites between an N-terminal Flag tag and a C-terminal nuclear-localization signal and MS2 coat protein. The identities of all constructs were confirmed by sequencing. PAC-1 cells were transfected with 500 ng splicing-reporter plasmid and 60 ng effector plasmid (or 200 and 100 ng, respectively, for **Fig. 5**). Expression of fusion proteins was monitored by western blotting using mouse monoclonal anti-Flag (M2) (Sigma) and secondary donkey anti-mouse conjugated to horseradish peroxidase. Rabbit polyclonal anti-ERK (Santa Cruz Biotechnology) was used as a loading control. RNA was detected by reverse-transcription (RT)-PCR using a $^{32}$P 5′ end–labeled PCR primer. PCR products were separated on denaturing polyacrylamide gels and quantitated by phosphorimaging using ImageQuant software[28]. Pull-downs of *in vitro*–translated protein by GST-PTB were carried out as described[28] using either GST alone or GST-SXL as negative controls. GST-SXL protein was produced from the plasmid pGEX CS NR SXL XW II, which was a kind gift from J. Valcárcel, Centre de Regulació Genòmica. RNase treatment of pull-downs was carried out in two steps: the *in vitro* translations were terminated with a 15-min incubation at 30 °C with 25 μg ml$^{-1}$ RNase A, and RNase A was added at 0.5 μg ml$^{-1}$ to the pull-down preincubation for 3 h at 4 °C.

**FRET measurements.** HeLa cells were plated onto HCl-treated coverslips 24 h before cotransfection with equal amounts of PTB and Raver1 constructs using Lipofectamine 2,000 (Invitrogen). After approximately 24 h, cells were fixed with 4% (v/v) formaldehyde and mounted with ProLong Gold antifade mounting medium (Molecular Probes). As a control, CFP-PTB and wild-type YFP-Raver1 were expressed independently.

To measure FRET, three images were acquired: (i) YFP channel ($I^{YFP}$; excitation 500/20 nm, emission 535/30 nm), (ii) CFP channel ($I^{CFP}$; excitation 430/25 nm, emission 470/30 nm) and (iii) FRET channel ($I^{FRET}$; excitation 430/25 nm, emission 535/30 nm). FRET sequences were obtained with an automated Olympus IX70 microscope equipped with a Sutter DG4 (175-W xenon lamp) allowing us to switch between different excitation wavelengths, a 60× 1.4 NA oil immersion objective and a filter wheel in the emission light path. The images were acquired with a cooled SensiCam QE CCD camera (Cooke Corp.) with no binning. To use the whole dynamic range of the CCD camera, the CFP and FRET images were acquired with an exposure time of 2 s and the YFP image with 1-s exposure time. All images were corrected for background fluorescence and registered to ensure accurate pixel alignment before carrying out the following FRET calculations.

The FRET signal was extracted from the FRET channel as described[43] and normalized for different expression levels[30]. Briefly, when FRET occurs, the donor fluorescence is decreased and the acceptor emission is increased (sensitized emission), but only a fraction of the donor (CFP) transfers energy to the acceptor (YFP). Most of the donor emits a photon and can bleed through the FRET channel. Additionally, YFP can be excited directly through the CFP excitation filter. Thus, the intensity of the fluorescence observed in the FRET channel ($I^{FRET}$) consists of a FRET component (cFRET) and a non-FRET component (CFP bleedthrough ($cF^{CFP} \times I^{CFP}$) and YFP direct excitation ($cF^{YFP} \times I^{YFP}$)):

$$I^{FRET} = cFRET + cF^{CFP} \times I^{CFP} \times cF^{YFP} \times I^{YFP} \quad (1)$$

where the cross-talk correction factor $cF^{CFP} = I_D^{FRET}/I_D^{CFP}$ and $cF^{YFP} = I_A^{FRET}/I_A^{YFP}$, D and A being donor- and acceptor-only samples, respectively.

$cF^{CFP}$ and $cF^{YFP}$ were determined from cells expressing only CFP-PTB or YFP-tagged wild-type Raver1, using the same experimental setup and exposure times as in the FRET experiments. Under our conditions, $cF^{CFP}$ and $cF^{YFP}$ were 0.58 ± 0.02 and 0.065 ± 0.015, respectively. Therefore, taking into account the cross-talk, CFP and YFP images multiplied by 0.60 and 0.08, respectively (average + s.d.), were subtracted from the FRET-channel image to calculate cFRET.

cFRET is intensity dependent. To compare different experiments and expression levels, the cFRET image was normalized according to equation (2). Normalized FRET (nFRET) is concentration independent[30].

$$nFRET = \frac{cFRET}{\sqrt{I^{CFP} \cdot I^{YFP}}} \quad (2)$$

Finally, from the YFP image, a binary mask was generated with values of 1 within the cell and 0 for the background. We multiplied cFRET and nFRET images by this binary mask to eliminate the background noise and kept the pixel

intensities unchanged within the cell. Acquisition was done with IP Lab version 3.51 (Scanalytics) and the images processed with ImageJ 1.33 (US National Institutes of Health).

**Peptides and protein constructs for NMR studies.** Plasmids expressing PTB1-1234, PTB1-12, PTB1-23, PTB1-34 and PTB1-2 have been described[5,6]. Plasmids for PTB1-2L (residues 147–334) and PTB4-2L (residues 147–360) were generated by PCR from full-length human PTB1 and human PTB4, respectively. These constructs differ only in the presence of a 26-residue insertion in PTB4-2L (after residue 298 of PTB1) in the RRM2-RRM3 linker region. DNA was ligated into the BamHI and HindIII sites of pQE9 (Qiagen), resulting in the addition of an uncleavable N-terminal His tag. Proteins were expressed as described[5,6] and purified on TALON resin (Clontech). Peptides for titration were synthesized using standard Fmoc chemistry (Advanced Biotechnology Centre, Imperial College London). A sample of N-terminally spin-labeled Raver1$_{499–506}$ peptide was prepared by reaction with the amine-reactive spin label 1-oxyl-2,2,5,5-tetramethylpyrroline-3-carboxylate *N*-hydroxysuccinimide ester (Toronto Research Chemicals) using the published protocol[44].

**NMR spectroscopy.** NMR spectra were recorded at 303 K on a 500-MHz four-channel Bruker DRX500 spectrometer equipped with a z-shielded gradient triple resonance cryo-probe. NMR data were processed using NMRPipe[45] and visualized with NMRView 4.1.3 (ref. 44).

**NMR titrations.** Samples of PTB for titration were typically 50–250 μM in 50 mM sodium phosphate buffer (pH 6.5), 150 mM NaCl, 10 mM DTT and 2 mM $NaN_3$. Raver1 peptide solutions were prepared by dissolving lyophilized peptide in identical buffer to 10–25 mM and the pH was adjusted to match that of the protein solution. The RNA oligonucleotide 5′-CUUCUCUCU-3′ (Dharmacon) was prepared similarly at 1.8 mM. For detection of binding to constructs of PTB1-1234, PTB1-12 and PTB1-34, $^{1}$H-$^{15}$N HSQC spectra were recorded in the absence and presence of a 20-fold excess of Raver1$_{491–511}$ peptide. Titrations of PTB1-2, PTB1-12, PTB1-23, PTB1-2L and PTB4-2L with Raver1$_{491–511}$, Raver1$_{491–511}$(L500A), Raver1$_{499–506}$ and Raver1$_{353–371}$ typically involved the stepwise addition of up to 100 molar equivalents of ligand over seven to ten points. Ligand additions for titration of the PTB1-2–Raver1$_{491–511}$ complex with RNA were of the following increments: 0, 0.3, 0.6, 1.0, 2.0 and 5.0 molar equivalents. Shift changes were monitored by 1D $^{1}$H and 2D $^{1}$H-$^{15}$N HSQC spectra and fit to a single–binding site saturation isotherm in Excel 2003 (Microsoft).

**1:1 RRM2–Raver1 complex.** For NMR spectra of the PTB1 RRM2–Raver1 peptide complex, a solution of Raver1 peptide uniformly $^{15}$N,$^{13}$C-labeled at residues equivalent to positions 499–505 (inclusive) was mixed with unlabeled RRM2 to an equimolar ratio and a final concentration of ~750 μM. Free peptide $^{1}$H assignments were obtained using 2D homonuclear TOCSY and NOESY spectra and extrapolated to the bound state by monitoring shift changes in $^{1}$H-$^{15}$N and $^{1}$H-$^{13}$C HSQC spectra. NOEs between the Raver1 peptide and RRM2 were measured in a standard $^{15}$N-separated NOESY-HSQC spectrum (200 ms mixing time) run with and without heteronuclear decoupling in the indirect $^{1}$H dimension to distinguish intra- from intermolecular NOEs. A spectrum after lyophilization and resuspension in 100% $D_2O$ was also acquired.

**RRM2–Raver1 peptide model.** Docking of the 496-PGVSLLGAPPKD-507 peptide to the minimized average NMR structure of PTB1 RRM2[6] used the HADDOCK protocol[32]. We generated 2,000 starting structures for the initial rigid-body minimization, from which 1,000 were selected for subsequent simulated annealing. During the simulated annealing and subsequent water-refinement stage, amino acid side chains within the putative binding site and the backbone of residues 193–196 (loop β1-α1) and 244–251 (loop α2-β4), inclusive, were allowed complete flexibility. The entire Raver1 peptide was also allowed complete flexibility during the calculation. We selected 200 lowest-energy simulated annealing models for a final water-refinement stage. AIR restraints were derived in standard fashion from chemical shift changes on the protein (ten) and peptide (seven) upon complex formation and supplemented with 11 intermolecular NOE restraints. All AIR and NOE restraint upper bounds were set to 5 Å. NOEs to RRM2 from the peptide were implemented ambiguously to circumvent reassignment of RRM2 in the complex. Ambiguity was reduced by conservative filtering of the restraints on the basis of the maximum change in chemical shift observed in the titration experiments and also the distance from the binding site. Separate experiments recorded in 90%/10% $H_2O/D_2O$ and 100% $D_2O$ were used to distinguish between NOEs to amide and aromatic side chain protons.

*Note: Supplementary information is available on the Nature Structural & Molecular Biology website.*


## ACKNOWLEDGMENTS

We thank J. Valcárcel for helpful comments on the manuscript, B. Jockusch for Raver1 monoclonal antibodies and I. Moss, of the Advanced Biotechnology Centre, Imperial College London, for technical advice and for preparation of the peptides. This work was funded by Wellcome Trust program grant 059879 to C.W.J.S. A.P.R. was supported by a Wellcome Trust Prize studentship. S.M. and S.C. are also indebted to the Wellcome Trust for grant support (078209). S.H. and M.L. were supported by US National Institutes of Health grant AR 41480 to R.H.S.


## AUTHOR CONTRIBUTIONS

A.P.R. mapped the Raver1 repressor domain and identified and characterized the PTB-interacting motif. C.G. did pull-down experiments identifying multiple PTB-interacting segments of Raver1, and some transfections. C.W.J.S. directed these experiments, coordinated the collaborations and wrote the first draft of the manuscript. S.M. and S.C. coordinated design of structural experiments. T.P.M. expressed and purified all PTB constructs; P.J.S. and S.M. planned and executed NMR experiments and data analysis. R.H.S. coordinated the FRET experiments. S.H. tested FRET with full-length Raver1. M.L. carried out all other FRET experiments. All authors contributed to writing and redrafting the manuscript.

## COMPETING INTERESTS STATEMENT

The authors declare that they have no competing financial interests.


Published online at http://www.nature.com/nsmb/
Reprints and permissions information is available online at http://npg.nature.com/reprintsandpermissions/



1. Lareau, L.F., Green, R.E., Bhatnagar, R.S. & Brenner, S.E. The evolving roles of alternative splicing. *Curr. Opin. Struct. Biol.* **14**, 273–282 (2004).
2. Cartegni, L., Chew, S.L. & Krainer, A.R. Listening to silence and understanding nonsense: exonic mutations that affect splicing. *Nat. Rev. Genet.* **3**, 285–298 (2002).
3. Matlin, A.J., Clark, F. & Smith, C.W. Understanding alternative splicing: towards a cellular code. *Nat. Rev. Mol. Cell Biol.* **6**, 386–398 (2005).
4. Wagner, E.J. & Garcia-Blanco, M.A. Polypyrimidine tract binding protein antagonizes exon definition. *Mol. Cell. Biol.* **21**, 3281–3288 (2001).
5. Conte, M.R. *et al.* Structure of tandem RNA recognition motifs from polypyrimidine tract binding protein reveals novel features of the RRM fold. *EMBO J.* **19**, 3132–3141 (2000).
6. Simpson, P.J. *et al.* Structure and RNA interactions of the N-terminal RRM domains of PTB. *Structure* **12**, 1631–1643 (2004).
7. Oberstrass, F.C. *et al.* Structure of PTB bound to RNA: specific binding and implications for splicing regulation. *Science* **309**, 2054–2057 (2005).
8. Perez, I., Lin, C.H., McAfee, J.G. & Patton, J.G. Mutation of PTB binding sites causes misregulation of alternative 3′ splice site selection *in vivo*. *RNA* **3**, 764–778 (1997).
9. Amir-Ahmady, B., Boutz, P.L., Markovtsov, V., Phillips, M.L. & Black, D.L. Exon repression by polypyrimidine tract binding protein. *RNA* **11**, 699–716 (2005).
10. Shen, H., Kan, J.L., Ghigna, C., Biamonti, G. & Green, M.R. A single polypyrimidine tract binding protein (PTB) binding site mediates splicing inhibition at mouse IgM exons M1 and M2. *RNA* **10**, 787–794 (2004).
11. Izquierdo, J.M. *et al.* Regulation of Fas alternative splicing by antagonistic effects of TIA-1 and PTB on exon definition. *Mol. Cell* **19**, 475–484 (2005).
12. Wagner, E.J. & Garcia-Blanco, M.A. RNAi-mediated PTB depletion leads to enhanced exon definition. *Mol. Cell* **10**, 943–949 (2002).
13. Gooding, C., Roberts, G.C. & Smith, C.W. Role of an inhibitory pyrimidine element and polypyrimidine tract binding protein in repression of a regulated alpha-tropomyosin exon. *RNA* **4**, 85–100 (1998).
14. Lin, C.H. & Patton, J.G. Regulation of alternative 3′ splice site selection by constitutive splicing factors. *RNA* **1**, 234–245 (1995).
15. Singh, R., Valcarcel, J. & Green, M.R. Distinct binding specificities and functions of higher eukaryotic polypyrimidine tract-binding proteins. *Science* **268**, 1173–1176 (1995).
16. Chou, M.Y., Underwood, J.G., Nikolic, J., Luu, M.H. & Black, D.L. Multisite RNA binding and release of polypyrimidine tract binding protein during the regulation of c-src neural-specific splicing. *Mol. Cell* **5**, 949–957 (2000).

17. Perez, I., McAfee, J.G. & Patton, J.G. Multiple RRMs contribute to RNA binding specificity and affinity for polypyrimidine tract binding protein. *Biochemistry* **36**, 11881–11890 (1997).
18. Oh, Y.L. *et al.* Determination of functional domains in polypyrimidine-tract-binding protein. *Biochem. J.* **331**, 169–175 (1998).
19. Monie, T.P. *et al.* The polypyrimidine tract binding protein is a monomer. *RNA* **11**, 1803–1808 (2005).
20. Zhang, W., Liu, H., Han, K. & Grabowski, P.J. Region-specific alternative splicing in the nervous system: implications for regulation by the RNA-binding protein NAPOR. *RNA* **8**, 671–685 (2002).
21. Charlet-B., N., Logan, P., Singh, G. & Cooper, T.A. Dynamic antagonism between ETR-3 and PTB regulates cell type-specific alternative splicing. *Mol. Cell* **9**, 649–658 (2002).
22. Gromak, N., Matlin, A.J., Cooper, T.A. & Smith, C.W. Antagonistic regulation of alpha-actinin alternative splicing by CELF proteins and polypyrimidine tract binding protein. *RNA* **9**, 443–456 (2003).
23. Polydorides, A.D., Okano, H.J., Yang, Y.Y., Stefani, G. & Darnell, R.B. A brain-enriched polypyrimidine tract-binding protein antagonizes the ability of Nova to regulate neuron-specific alternative splicing. *Proc. Natl. Acad. Sci. USA* **97**, 6350–6355 (2000).
24. Markovtsov, V. *et al.* Cooperative assembly of an hnRNP complex induced by a tissue-specific homolog of polypyrimidine tract binding protein. *Mol. Cell. Biol.* **20**, 7463–7479 (2000).
25. Yamamoto, H., Tsukahara, K., Kanaoka, Y., Jinno, S. & Okayama, H. Isolation of a mammalian homologue of a fission yeast differentiation regulator. *Mol. Cell. Biol.* **19**, 3829–3841 (1999).
26. Gooding, C., Kemp, P. & Smith, C.W. A novel polypyrimidine tract-binding protein paralog expressed in smooth muscle cells. *J. Biol. Chem.* **278**, 15201–15207 (2003).
27. Huttelmaier, S. *et al.* Raver1, a dual compartment protein, is a ligand for PTB/hnRNPI and microfilament attachment proteins. *J. Cell Biol.* **155**, 775–786 (2001).
28. Gromak, N. *et al.* The PTB interacting protein raver1 regulates alpha-tropomyosin alternative splicing. *EMBO J.* **22**, 6356–6364 (2003).
29. Robinson, F. & Smith, C.W.J. A splicing repressor domain in polypyrimidine tract binding protein. *J. Biol. Chem.* **281**, 800–806 (2006).
30. Xia, Z. & Liu, Y. Reliable and global measurement of fluorescence resonance energy transfer using fluorescence microscopes. *Biophys. J.* **81**, 2395–2402 (2001).
31. Hahm, B. *et al.* Polypyrimidine tract-binding protein interacts with HnRNP L. *FEBS Lett.* **425**, 401–406 (1998).
32. Dominguez, C., Boelens, R. & Bonvin, A.M. HADDOCK: a protein-protein docking approach based on biochemical or biophysical information. *J. Am. Chem. Soc.* **125**, 1731–1737 (2003).
33. Singh, R. & Valcarcel, J. Building specificity with nonspecific RNA-binding proteins. *Nat. Struct. Mol. Biol.* **12**, 645–653 (2005).
34. Selenko, P. *et al.* Structural basis for the molecular recognition between human splicing factors U2AF65 and SF1/mBBP. *Mol. Cell* **11**, 965–976 (2003).
35. Sharma, S., Falick, A.M. & Black, D.L. Polypyrimidine Tract Binding protein blocks the 5′ splice site dependent assembly of U2AF and the prespliceosomal E complex. *Mol. Cell* **19**, 485–496 (2005).
36. Chan, D.C., Bedford, M.T. & Leder, P. Formin binding proteins bear WWP/WW domains that bind proline-rich peptides and functionally resemble SH3 domains. *EMBO J.* **15**, 1045–1054 (1996).
37. Bedford, M.T., Chan, D.C. & Leder, P. FBP WW domains and the Abl SH3 domain bind to a specific class of proline-rich ligands. *EMBO J.* **16**, 2376–2383 (1997).
38. Bedford, M.T., Reed, R. & Leder, P. WW domain-mediated interactions reveal a spliceosome-associated protein that binds a third class of proline-rich motif: the proline glycine and methionine-rich motif. *Proc. Natl. Acad. Sci. USA* **95**, 10602–10607 (1998).
39. Wollerton, M.C., Gooding, C., Wagner, E.J., Garcia-Blanco, M.A. & Smith, C.W. Autoregulation of polypyrimidine tract binding protein by alternative splicing leading to nonsense-mediated decay. *Mol. Cell* **13**, 91–100 (2004).
40. Roberts, G.C., Gooding, C., Mak, H.Y., Proudfoot, N.J. & Smith, C.W. Co-transcriptional commitment to alternative splice site selection. *Nucleic Acids Res.* **26**, 5568–5572 (1998).
41. Tian, M. & Maniatis, T. A splicing enhancer exhibits both constitutive and regulated activities. *Genes Dev.* **8**, 1703–1712 (1994).
42. Kleinhenz, B. *et al.* Raver2, a new member of the hnRNP family. *FEBS Lett.* **579**, 4254–4258 (2005).
43. Gordon, G.W., Berry, G., Liang, X.H., Levine, B. & Herman, B. Quantitative fluorescence resonance energy transfer measurements using fluorescence microscopy. *Biophys. J.* **74**, 2702–2713 (1998).
44. Johnson, B.A. & Blevins, R.A. NMRVIEW—a computer program for the visualization and analysis of NMR data. *J. Biomol. NMR* **4**, 603–614 (1994).
45. Delaglio, F. *et al.* NMRPipe: a multidimensional spectral processing system based on UNIX pipes. *J. Biomol. NMR* **6**, 277–293 (1995).